IEEE Access
Multidisciplinary | Rapid Review | Open Access Journal

Received 10 January 2023, accepted 26 January 2023, date of publication 6 February 2023, date of current version 9 February 2023.

Digital Object Identifier 10.1109/ACCESS.2023.3242684

RESEARCH ARTICLE

Accurate Estimation of LPI Radar Pulse Train Parameters via Change Point Detection

JONG-HYEON BANG[1], (Graduate Student Member, IEEE), DO-HYUN PARK[1], (Graduate Student Member, IEEE), WONJIN LEE[2], DOOHWAN KIM[2], AND HYOUNG-NAM KIM[1], (Member, IEEE)

[1]Department of Electronics Engineering, Pusan National University, Busan 46241, Republic of Korea
[2]LIG Nex1, Seongnam-si 13488, Republic of Korea

Corresponding author: Hyoung-Nam Kim (hnkim@pusan.ac.kr)

This work was supported by the Korea Research Institute for Defense Technology Planning and Advancement-Grant funded by Defense Acquisition Program Administration (DAPA) under Grant KRIT-CT-21-033.

ABSTRACT Estimating the time of arrival (TOA), pulse width (PW), and pulse repetition interval (PRI) is critical for identifying the low probability of intercept (LPI) radar signals as it is common in electronic warfare (EW) to experience a pulse train being received. To determine these parameters, we need to differentiate between pulse and noise in a pulse train. However, separating the LPI radar pulse train into pulse and noise is challenging owing to its characteristics and modulation scheme. Therefore, we propose a method to accurately estimate TOA, PW, and PRI using change point detection, which can effectively classify the pulse train into pulse and noise. The main contributions of this study are as follows. First, a denoising method robust to various modulation schemes is introduced. Second, an algorithm capable of estimating the parameters without considering the threshold calculation is presented. Moreover, most prior studies have entailed parameter estimations for a single pulse. In contrast, we focus on estimating parameters when a pulse train is intercepted and generating superior results even in the signal-to-noise ratio under 0 dB. We present experiments performed on the following eight modulation schemes: linear frequency modulation, Costas, Barker, Frank, P1, P2, P3, and P4 codes. Furthermore, we compare the proposed method with the wavelet-based method, which has received much attention in EW. The results demonstrate that the proposed method outperforms the conventional approaches.

INDEX TERMS Electronic warfare, LPI radar signal, parameter estimation, change point detection.

I. INTRODUCTION

Many radar emitters widely use low probability of intercept (LPI) signals to prevent an opponent receiver from intercepting and detecting their emissions [1]. As the LPI radar signal is not intended to be identified by the electronic warfare support (ES) receiver, it has a low peak power, low signal-to-noise ratio (SNR), high duty cycle, and large bandwidth [1], [2]. As a result, the development of various countermeasures for identifying LPI radar signals has been accelerated, such as localization of radar [3], deinterleaving of pulse train [4], waveform recognition [5], and artificial intelligence techniques [6] in ES systems.

The associate editor coordinating the review of this manuscript and approving it for publication was Brian Ng.

In general, the ES systems sequentially perform detection and analysis of the intercepted signal to recognize the enemy's threat. It is important to estimate the signal parameters to analyze the opponent's signal source. Time of arrival (TOA), pulse width (PW), and pulse repetition interval (PRI) are commonly considered as key parameters among them [7], and threats are perceived by comparing the estimated parameters with the pre-stored data in electronic intelligence [8]. The processed information is immediately transmitted to the friendly forces, assisting in the development of effective tactical strategies and the quick decision of countermeasures. Therefore, successful acquisition of the enemy's signal information is a prerequisite for the operation of EW systems.

Many estimation methods have been studied to collect meaningful data from the received signal. TOA, PW, and

PRI estimation methods based on an envelope detector and dual decision thresholds were introduced in [9] and [10]. As the radar signals are strongly affected by the noise due to power loss caused by free-space path loss, most of them have low SNRs of less than 0 dB. Therefore, these approaches are fragile in such a weak-signal environment. A modified Wigner–Ville distribution (WVD) that eliminates all interferences and smoothens the waveform's rough edges was presented in [11]. The signal is transformed into a time-frequency representation by employing the modified WVD, and an instantaneous power in time-frequency analysis and a threshold are used to find the PW and PRI. However, only linear frequency modulation (LFM) was considered. In [12], a cross-correlation-based two-stage PW estimation method was proposed for binary phase shift keying (BPSK). In the first stage, the center frequency is estimated by conducting the cross-correlation between the received and the reference signals. In the second stage, the PW is extracted by cross-correlation between them, having the estimated center frequency in the first stage. Although this method can determine the parameters in a high-noise environment, performance degradation arises when the center frequency of the received signal does not match with the reference signal. In addition, only BPSK was considered. In [13], the time-frequency analysis produced from the smooth pseudo-Wigner–Ville distribution is converted into a binary map, and the PW is determined by projecting the binary map onto the time axis. However, the performance deteriorates when an overlap occurs between the Costas sequences in the time axis. A PW estimation method based on edge detection, which utilizes a Haar filter and a threshold, was presented in [14]. However, a weak-signal environment was not considered.

In addition, a study on wavelet denoising has also drawn considerable attention in EW. The estimation method employing wavelet packet decomposition and kurtosis enhanced the pulse amplitude estimation accuracy by determining the exact PW [15]. As a threshold based on kurtosis is used to decide the presence of noise in each packet, it is suitable for a signal with an SNR of upper 0 dB. Noise reduction via Gaussian wavelet increased the SNR of the received signal by choosing the wavelet coefficient with the maximum power ratio [16]. However, this method is only applicable to the low-frequency band, and the filter gain is not flat. The modified sinc wavelet addressed in [17] overcame the disadvantages of the existing mother wavelet and improved the SNR of the signal received in a wide range of frequency bands through the wavelet transform. However, these wavelet transform-based studies focus only on signal detection by mitigating the noise. The crucial role of the ES systems is to detect and analyze the opponent's threat.

Since the 1950s, there has been substantial interest in the study of change point detection (CPD) in a variety of fields [18]. CPD aims to identify points in real-time series data where a significant statistical change occurs. CPD was used to monitor human health behavior and status by locating change points in the electroencephalogram signal [19]. Moreover, applying CPD to speech signal processing improved the segmentation of entire audio tracks from TV shows as well as speaker diarization [20]. CPD has been actively utilized in diverse signal processing fields but has yet to be used in EW signal processing.

This paper proposes an estimation method of the TOA, PW, and PRI for the LPI radar pulse train based on CPD. The proposed method comprises two steps—denoising and estimation. A tailor-made sinc filter for the intercepted signal is designed using CPD in the denoising step. We can acquire the denoised pulse train through the designed optimal sinc filter. After suppressing the noise, the pulse train is split into several segments by CPD. Then, we combined the segment's mean and variance into 2-D data and used the K-means algorithm on these data to determine whether a segment is a pulse or noise. Consequently, we allocated 0 for the noise segment and 1 for the pulse segment based on the classified result and estimated the TOA, PW, and PRI by selecting any threshold between 0 and 1.

The main contribution of this study is that it provides an accurate estimation method for the TOA, PW, and PRI in a weak-signal environment. In addition, most studies have not considered various modulation schemes [9], [10], [11], [12], [13], [14], [15], [16], [17], whereas the proposed method shows robust estimation performance for the eight modulation schemes, such as LFM, Costas, Barker, Frank, P1, P2, P3, and P4 codes. Furthermore, most threshold-based estimation methods use a fixed value or a variable value (e.g., constant false alarm rate) as a threshold [9], [10], [11], [14], [15]. However, fixed-threshold-based methods are vulnerable in coping with a weak-signal environment because the noise is dominant as SNR decreases. The estimation performance of variable-threshold-based methods depends on many parameters, such as the probability of false alarms, number of reference cells, and number of guard cells [21]. To minimize these potential troubles, we take a different approach of separating the pulse train into pulse and noise in advance and then using a fixed threshold. Lastly, most studies consider single pulses [12], [13], [14], [15], [16]. Although some studies concentrate on parameter estimation for the pulse train, they are fragile to weak signals [9], [10] or consider only single modulation [11]. In this study, we focused on overcoming these drawbacks when the pulse train is intercepted.

The remainder of this paper is organized as follows. Section II briefly reviews an LPI radar signal model, a CPD exploited in the proposed method, and the K-means algorithm. Section III describes the proposed TOA, PW, and PRI estimation method based on CPD. In Section IV, the performance of the proposed method is compared with those of the existing methods based on wavelet transform using the experimental results. Section V provides the conclusions drawn from this study.

TABLE 1. LPI radar waveform.

Radar waveform	$f[n]$ [Hz]	$\phi[n]$ [rad]
LFM	$f_0 + \frac{B}{\tau_{pw}}(nT_s)$	constant
Costas	f_i	constant
Barker	constant	0 *or* π
Frank	constant	$\frac{2\pi}{M}(i-1)(j-1)$
P1	constant	$-\frac{\pi}{M}[M-(2j-1)][(j-1)M+(i-1)]$
P2	constant	$-\frac{\pi}{2M}[2i-1-M][2j-1-M]$
P3	constant	$\frac{\pi}{N_c}(i-1)^2$
P4	constant	$\frac{\pi(i-1)^2}{N_c}-\pi(i-1)$

II. RELATED WORK

In this section, we first present a brief explanation of the eight LPI radar signals. Then, a CPD and a K-means algorithm, which are exploited in the proposed method, are introduced.

A. LPI RADAR SIGNAL MODEL

An intercepted LPI radar signal $y[n]$, including the discrete-time complex radar signal $s[n]$ and the complex additive white Gaussian noise (AWGN) $w[n]$, is defined as

$$y[n] = s[n] + w[n] = Ae^{j2\pi f[n](nT_s)+\phi[n]} + w[n], \quad (1)$$

where A is a complex amplitude which is constant within the pulse width τ_{pw} for $0 \le nT_s \le \tau_{pw}$, n is a sample index increasing every T_s for a sampling frequency, $f[n]$ is an instantaneous frequency, and $\phi[n]$ is a phase modulation function.

The LPI radar signal has three types: frequency modulation, phase modulation, and combined modulation [22]. In frequency modulation, the $\phi[n]$ is kept constant while the $f[n]$ is varied, whereas $f[n]$ is kept constant while the $\phi[n]$ is changed in phase modulation. Combined modulation is a combination of frequency and phase modulation. The eight modulation schemes used in this study are shown in Table 1. Here, B is the bandwidth of LFM, f_i is the Costas sequence, M is the number of frequency steps, $N_c = M^2$ is the compression ratio, and i, j denote the phase of the ith sample of the jth frequency.

B. CHANGE POINT DETECTION

CPD is an algorithm that detects points where a sudden statistical change appears in real-time series data and is used in diverse fields such as finance, climatology, network traffic analysis, signal processing, and speech processing [23]. The CPD is usually classified into two categories: constrained and penalized minimization problems.

1) CONSTRAINED MINIMIZATION PROBLEM

The constrained minimization problem restricts the optimization by fixing the maximum number of change points that can be found. If we know the maximum number of change points k, CPD finds $\tau_1, \tau_2, \ldots, \tau_k$ such that the following total cost function C_t is minimized [24].

$$C_t = \min_{\tau_{1:k}} \sum_{j=0}^{k} C\left(\mathbf{y}_{\tau_j+1:\tau_{j+1}}\right), \quad (2)$$

where $\mathbf{y} = (y_1, y_2, \ldots, y_n)$ is the all input data, $\mathbf{y}_{\tau_j+1:\tau_{j+1}} = (y_{\tau_j+1}, y_{\tau_j+2}, \ldots, y_{\tau_{j+1}})$ is the partial input data from τ_j+1 to τ_{j+1}, C is the cost function, $\tau = (\tau_0, \tau_1, \ldots, \tau_k, \tau_{k+1})$ is the set of change points, and $\tau_0 = 0$, $\tau_{k+1} = n$. The form of the cost function depends on the type of change we want to find. For instance, the cost function recognizing a drastic mean change is expressed as follows [24]:

$$C_{average} = \min_{\tau_{1:k}} \sum_{i=0}^{k} \left[\sum_{j=\tau_i+1}^{\tau_{i+1}} \left(y_j - \frac{1}{\tau_{i+1}-\tau_i} \sum_{l=\tau_i+1}^{\tau_{i+1}} y_l \right)^2 \right]. \quad (3)$$

2) PENALIZED MINIMIZATION PROBLEM

If the number of change points k is unknown, we must simultaneously determine the number and the position of the change points by solving a penalized minimization problem. Unlike the constrained minimization problem, the penalized minimization problem has a penalty constant β in the total cost function [24].

$$C_t = \min_{k,\tau_{1:k}} \sum_{j=0}^{k} \left[C\left(\mathbf{y}_{\tau_j+1:\tau_{j+1}}\right) + \beta \right]. \quad (4)$$

Several studies have been conducted in statistical signal processing to find the change points when the number of change points is unknown. Among them, a pruned exact linear time (PELT) shows high detection accuracy with low computational complexity [25]. Because of these advantages, we incorporate PELT to solve the penalized minimization problem in EW.

In the penalized minimization problem, choosing the optimal penalty constant is critical. If the penalty constant is too small, overfitting occurs in which unnecessary changes are detected. In contrast, if the penalty constant is too large, underfitting occurs in which the necessary changes are not recognized. Fig. 1(a) and (b) show random numbers with rapid mean changes at indices 11, 31, and 51 to give the example of overfitting and underfitting. As shown in Fig. 1(a), the change points found by PELT are more than necessary because the penalty constant is small. Although abrupt mean changes occurred at index 51 in Fig. 1(b), PELT cannot recognize it as the penalty constant is large. Therefore, the choice

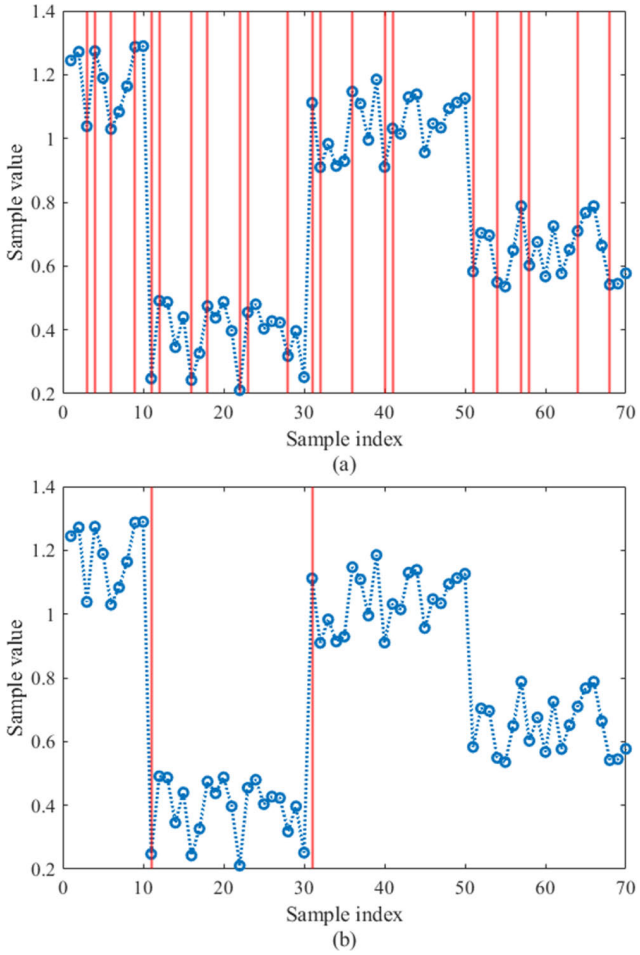

FIGURE 1. Examples of overfitting and underfitting in change point detection; (a) overfitting, (b) underfitting.

of the penalty constant is closely related to the detection accuracy.

3) CROPS METHOD

It is essential to pick the optimal penalty constant in the penalized minimization problem. The change points for a range of penalties (CROPS) is one of the algorithms to get the optimal penalty range [26]. The motivation of the CROPS is that there may exist a non-optimal number of change points when the cost and the number of change points are calculated according to the penalty constant by running CPD.

From this observation, CROPS decides whether the number of change points for the initial minimum and the maximum penalty range $[\beta_{min}, \beta_{max}]$ set by the user is optimal. If $[\beta_{min}, \beta_{max}]$ is optimal by satisfying certain conditions, we have divided the input into optimal segments for $\beta \in [\beta_{min}, \beta_{max}]$. Otherwise, $[\beta_{min}, \beta_{max}]$ is divided into $[\beta_{min}, \beta_{int}]$ and $[\beta_{int}, \beta_{max}]$, where β_{int} is the value between β_{min} and β_{max} defined from the theoretical results in [26]. This process is repeated for each $[\beta_{min}, \beta_{int}]$ and $[\beta_{int}, \beta_{max}]$ until an optimal penalty range is acquired. We can avoid overfitting or underfitting in the penalized minimization problem by using CROPS.

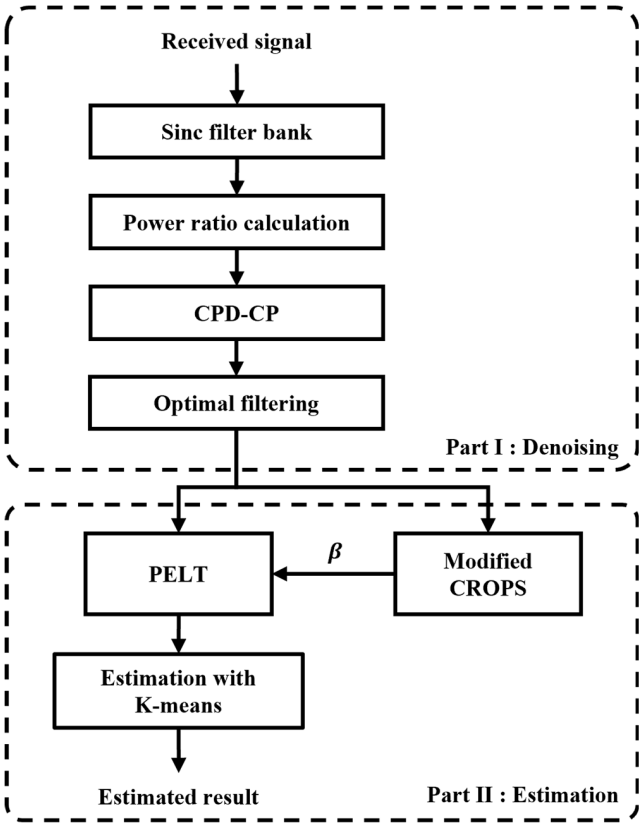

FIGURE 2. Block diagram of the proposed method.

C. K-MEANS ALGORITHM

K-means is an unsupervised learning algorithm widely employed in cluster analysis. It repeats the process of separating data using the nearest-centroid decision rule [27]. A brief outline of the K-means algorithm is as follows:

i) Randomly select the centroid of each K cluster.
ii) Assign data close to the centroid of each K cluster to the corresponding cluster.
iii) Update each centroid to the average position of the cluster.
iv) Repeat step 2 using the updated centroid.
v) Repeat steps 2 to 4 until the centroid converges.

III. SIGNAL PARAMETERS ESTIMATION BASED ON CHANGE POINT DETECTION

This section describes the proposed method based on CPD to estimate TOA, PW, and PRI. Fig. 2 shows the block diagram of the proposed method consisting of denoising and estimation parts. Each part incorporates a CPD to accomplish its purpose. K-means algorithm is exploited in the estimation part to distinguish between the pulse and noise. The details of each block are presented in the following subsections.

A. DENOISING STEP

1) POWER RATIO IN FREQUENCY DOMAIN

Assuming that the signal is stationary within the filter, the time-frequency representation $TFR(\tau, f)$ based on the sinc

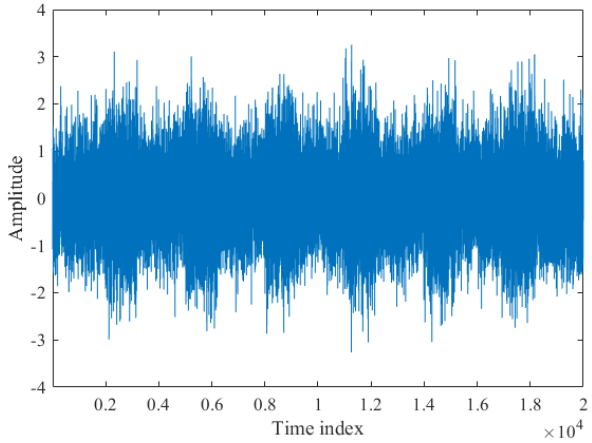

FIGURE 3. Received LFM signal when the SNR is 0 dB.

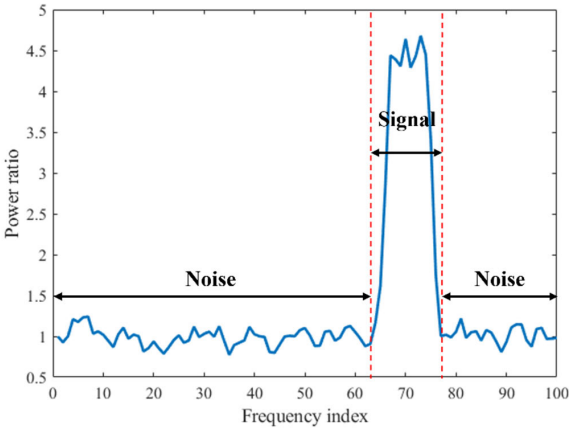

FIGURE 4. Power ratio of the LFM when the SNR is 0 dB.

filter bank is conducted by the inner products of a signal $x(t)$ and a sinc filter $w(t)$, which can be denoted as

$$TFR(\tau, f) = \int_{-\infty}^{\infty} x(t)\, w^*(t-\tau)\, dt, \tag{5}$$

where

$$w(t) = \frac{\sin(B\pi t)}{\pi t} e^{j2\pi ft}. \tag{6}$$

After producing the time-frequency analysis, the following power ratio $P(f)$ in the frequency axis is calculated to find the signal bandwidth [28].

$$P(f) = \frac{\int_{-\infty}^{\infty} \left|TFR_{signal}(\tau, f)\right|^2 d\tau}{E\left[\int_{-\infty}^{\infty} |TFR_{noise}(\tau, f)|^2 d\tau\right]}, \tag{7}$$

where $TFR_{signal}(\tau, f)$ and $TFR_{noise}(\tau, f)$ are the time-frequency analysis of the input signal and noise, respectively. Fig. 3 is a received LFM signal with the SNR of 0 dB. We can get the power ratio values corresponding to this signal by conducting the power ratio calculation, as shown in Fig. 4. The power ratio in the noise region is about 1, and the power ratio in the signal region is greater than 1. Due to this shape, we can get the signal bandwidth by applying CPD.

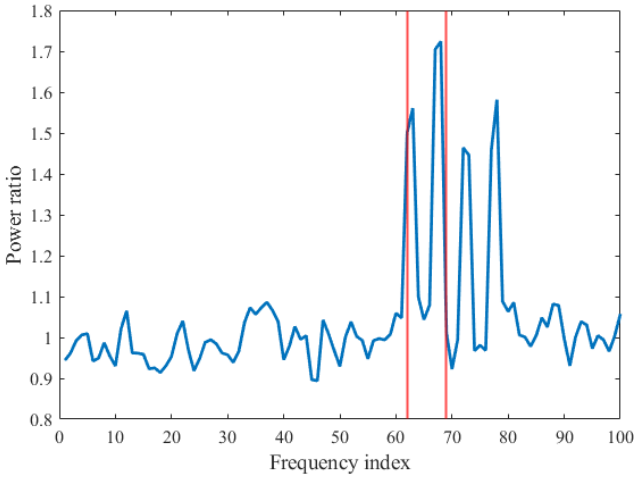

FIGURE 5. Change points detection result of the Costas code power ratio when the SNR is −5 dB.

We estimated the signal parameters with a single frequency component because a signal with multiple frequency components is deemed a deinterleaving problem before estimation [29]. A signal with a single frequency component has two change points in the power ratio: increasing and decreasing portions. Therefore, we considered this problem as a constrained minimization problem when applying CPD to the power ratio and fixed the maximum number of change points to 2.

2) CHANGE POINTS DETECTION WITH CUMULATIVE POWER RATIO

There are many modulation schemes of the LPI radar signal in EW. Unlike other modulation schemes, the Costas code has a frequency hopping sequence. There is a disadvantage when finding the change point in the power ratio because of this property. Fig. 5 shows the detection result of the Costas code power ratio having a frequency interval of 5 MHz and an SNR of −5 dB. Only two of the four hopping sequences were detected. This was because of the large gap between hopping sequences. In addition, as the amplitude of some hopping sequences increased owing to the influence of noise in low SNR, CPD might recognize these hopping sequences as abrupt statistical changes.

To overcome these shortcomings, we propose the change point detection with cumulative power ratio (CPD-CP), where CPD is conducted on the cumulative power ratio defined by

$$P_{cum}(f) = \sum_{f=1}^{n} (P(f) - 1)^2. \tag{8}$$

Here, n is the number of the filter bank. The insight of the CPD-CP is that the power ratio in the noise area is approximately 1. Accordingly, the cumulative power ratio has a shape in which the slope gradually increases in the noise section, whereas the slope surge in the signal section. This shape is optimal for detecting abrupt slope changes, and the cost

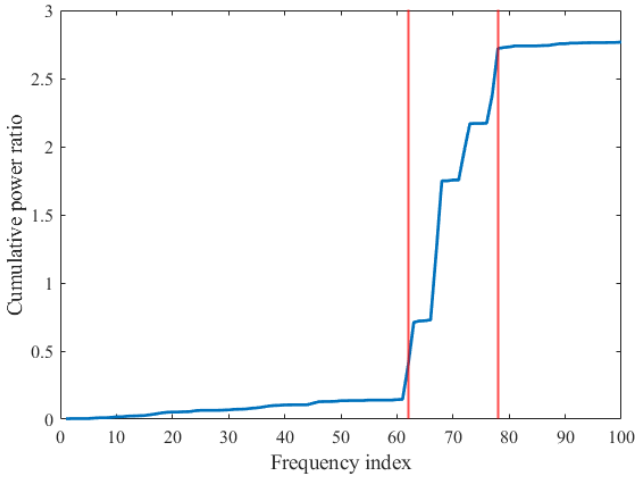

FIGURE 6. Detection result of the CPD-CP for the same Costas code in Fig. 5.

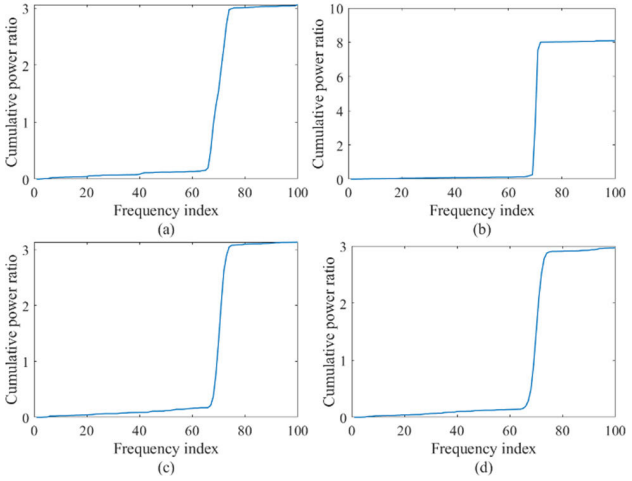

FIGURE 7. Cumulative power ratios when the SNR is −5 dB; (a) LFM, (b) Barker code, (c) Frank code, (d) P1 code.

function to recognize the slope change is as follows [30]:

$$\begin{aligned} C_{slope} &= \min_{\tau_{1:k}} \sum_{i=0}^{k} C\left(P_{cum}\left(\tau_i + 1 : \tau_{i+1}\right)\right) \\ &= \min_{\tau_{1:k}} \sum_{i=0}^{k} \left[\sum_{j=\tau_i+1}^{\tau_{i+1}} \left[P_{cum}\left(j\right) \right.\right. \\ &\quad \left.\left. - \left(\frac{\phi_{\tau_{i+1}} - \phi_{\tau_i}}{\tau_{i+1} - \tau_i} \left(j - \tau_i\right) - \phi_{\tau_i} \right) \right]^2 \right], \end{aligned} \tag{9}$$

where ϕ_{τ_i} is the value at the change point τ_i.

Fig. 6 represents the detection result of the CPD-CP for the same Costas code in Fig. 5. The upsurge in the signal region is prominent and can be detected well. In addition, the cumulative power ratio for the Costas code increases stepwise because of the hopping sequence. In contrast, the cumulative power ratio of the other modulation schemes increases linearly, as shown in Fig. 7. Here, the maximum value of the Barker code is larger than those of the others because its modulation bandwidth is narrower compared to the other modulation schemes. Furthermore, P2, P3, and P4 codes also have similar shapes. From this observation, we can determine the signal bandwidth for various modulation schemes through the CPD-CP.

3) OPTIMAL FILTERING

We can acquire two change points by performing CPD-CP on the power ratio, and these points are denoted as cp_{min} and cp_{max}. In addition, a margin ξ is added to get the signal bandwidth fully. After that, we can define the minimum and maximum values of the signal bandwidth as

$$\begin{aligned} B_{min} &= cp_{min} - \xi, \\ B_{max} &= cp_{max} + \xi. \end{aligned} \tag{10}$$

Then, the optimal sinc filter can be designed by

$$w\left(t\right) = \frac{\sin\left(\left(B_{max} - B_{min}\right)\pi t\right)}{\pi t} e^{j2\pi\left(\frac{B_{max}+B_{min}}{2}\right)t}. \tag{11}$$

Finally, we can mitigate the noise in the pulse train by passing through the designed filter. In conclusion, the proposed denoising step can suppress the noise of the LPI radar signal without distortion by setting the flexible filter bandwidth according to the signal bandwidth.

B. ESTIMATION STEP

1) MODIFIED CROPS

The denoised pulse train has an apparent statistical difference between the noise and the pulse signal. In this respect, we can divide the denoised pulse train into pulse and noise segments by applying CPD. However, we cannot know the number of pulses in the intercepted signal. Therefore, we consider this problem as a penalized minimization problem and apply PELT on the denoised pulse train. Because the penalty constant is a critical factor in determining the detection accuracy in PELT, we propose a modified CROPS (mCROPS) algorithm to acquire the optimal penalty range in EW efficiently.

Fig. 8 shows a snapshot of the number of change points k according to the penalty constant β from 0.5 to 9 for each modulation scheme. We can get these outcomes by performing PELT for varying β on a denoised pulse train having 6 pulses. As the number of pulses is 6, the ideal number of change points is 12. Fig. 8(a) is the snapshot when the PW is minimum in the practical PW range, and SNR is −5 dB. Fig. 8(b) represents the snapshot when the SNR of (a) is changed to 0 dB, and Fig. 8(c) shows the snapshot when the PW of (a) is altered to maximum. From these results, we arrive at the following four facts.

i) The optimal penalty range is different for each modulation scheme. For example, Costas code has an optimal penalty range at [1, 1.9], but Frank code at [3.1, 5.5] in Fig. 8(a).
ii) The optimal penalty range is dissimilar according to SNR and PW.
iii) In Fig. 8(a), as the penalty constant decreases, overfitting appears in some modulation schemes, but others may have an optimal. For instance, overfitting arises

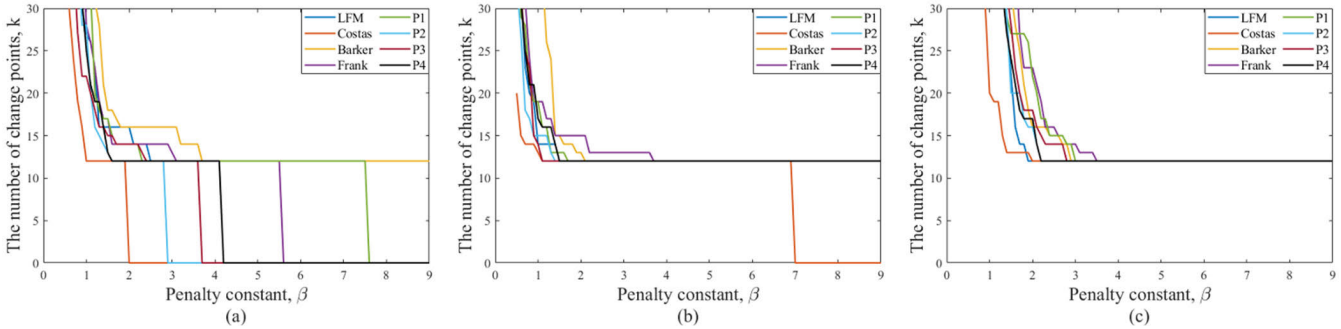

FIGURE 8. Snapshot for the number of change points according to the penalty constant; (a) SNR = −5 dB and minimum PW, (b) SNR = 0 dB and minimum PW, (c) SNR = −5 dB and maximum PW.

Algorithm 1 Modified CROPS Method

Input: $\mathbf{y} = (y_1, y_2, \ldots, y_n)$ where $y_i \in \mathbb{R}$
Initial penalty range, $[\beta_{min}, \beta_{max}]$
Interval of the initial penalty range, β_{inter}
Output: The details of optimal segmentations for each $\beta \in [\beta_{min}, \beta_{max}]$

for iteration $\beta = \beta_{min}, \beta_{min} + \beta_{inter}, \ldots, \beta_{max}$ **do**
  Run PELT for penalty value β
  if $k(\beta) = 0$ or 1 **then**
    Set $\beta_{max} = \beta - \beta_{inter}$
    break
  end
end
Run PELT for penalty values β_{min} and β_{max}
Set $\beta^* = \{[\beta_{min}, \beta_{max}]\}$
while $\beta^* \neq \emptyset$ **do**
  Choose an element of β^*; denote this element as $[\beta_0, \beta_1]$
  if $k(\beta_0) > k(\beta_1) + 1$ **then**
    Calculate $\beta_{int} = \frac{Q_{k(\beta_1)}(y_{1:n}) - Q_{k(\beta_0)}(y_{1:n})}{k(\beta_0) - k(\beta_1)}$
    Run PELT for penalty value β_{int}
    if $k(\beta_{int}) \neq k(\beta_1)$ **then**
      Set $\beta^* = \{\beta^*, [\beta_{int}, \beta_1]\}$
    end
  end
  Set $\beta^* = \beta^* \backslash [\beta_0, \beta_1]$
end

when the penalty constant is less than 1.6 in the P4 code, whereas it is optimal from 1 to 1.6 for the Costas code.

iv) When the signal is received, a penalty constant for which the number of change points is 0 or 1 is not required as at least two change points are needed for a single pulse.

From these insights, the mCROPS is presented in Algorithm 1 where $k(\beta)$ is the number of change points for β, and $Q_{k(\beta)}(\mathbf{y}_{1:n})$ is the cost of having k change points when running PELT for β on input data $\mathbf{y}_{1:n}$.

At the beginning of the mCROPS, PELT is run for every interval β_{inter} within the initial penalty range $[\beta_{min}, \beta_{max}]$ on the denoised pulse train. We can acquire the maximum penalty constant before k becomes 0 or 1 from this process. This penalty constant is again set to β_{max}, and PELT is performed for β_{min} and β_{max}. Then if $k(\beta_{min}) \leq k(\beta_{max}) + 1$, we find all the optimal segmentations for $\beta \in [\beta_{min}, \beta_{max}]$. Otherwise, we calculate β_{int} and run PELT for β_{int}. Then if $k(\beta_{int}) = k(\beta_{max})$, we obtain all optimal segments for $\beta \in [\beta_{min}, \beta_{max}]$. Otherwise, we consider the range of $[\beta_{int}, \beta_{max}]$ and repeat this procedure in this range. This continues until there is no new penalty range to consider.

There are two distinctions between CROPS and mCROPS. First, the penalty constant before the number of change points becomes 0 or 1 is set to the β_{max}. Second, if $[\beta_{min}, \beta_{max}]$ is not optimal, the overall process is repeated for $[\beta_{int}, \beta_{max}]$ instead of $[\beta_{min}, \beta_{int}]$ and $[\beta_{int}, \beta_{max}]$. These modifications prevent the algorithm from running in an unnecessary penalty range and avoid undesirable consequences in advance. For example, the Costas, P3, and Barker codes in Fig. 8(a) have optimal penalty ranges [1, 1.9], [2.4, 3.6], and [3.7, 9], respectively. In this case, we should consider setting 1 to 9 as the initial penalty range because we cannot know the modulation scheme of the intercepted signal. However, the penalty range [3.7, 9], which is optimal for the Barker code, is meaningless for the Costas and the P3 codes as their number of change points is 0. In addition, the P3 and the Barker codes do not require PELT to run for $\beta < 2$ owing to overfitting, whereas the Costas code does. In this sense, mCROPS extracts the appropriate penalty range in EW more efficiently and the computational cost is also naturally reduced by these changes.

Fig. 9 shows the detection result of the PELT with mCROPS in a denoised pulse train with an SNR of −5 dB, where 13 segments appear. Among these segments, we have to decide which part is noise or pulse during the signal processing. To achieve this goal and find the required parameters, we propose an estimation procedure with a K-means algorithm.

2) ESTIMATION WITH K-MEANS

After segmentation by PELT with mCROPS, we can calculate each segment's mean and variance. Fig. 10 shows the segment's mean and variance determined from the result in Fig. 9. The noise segment has a relatively smaller value than the pulse segment. Based on this observation, we have developed the following estimation algorithm: estimation with K-means.

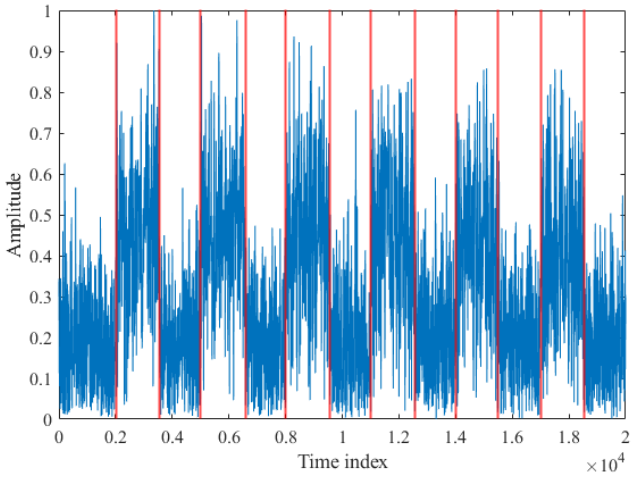

FIGURE 9. Detection result of the PELT with the modified CROPS.

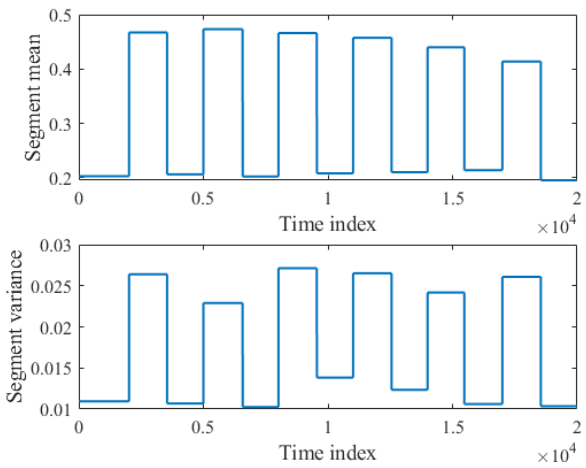

FIGURE 10. Segment mean and variance calculated from Fig. 9.

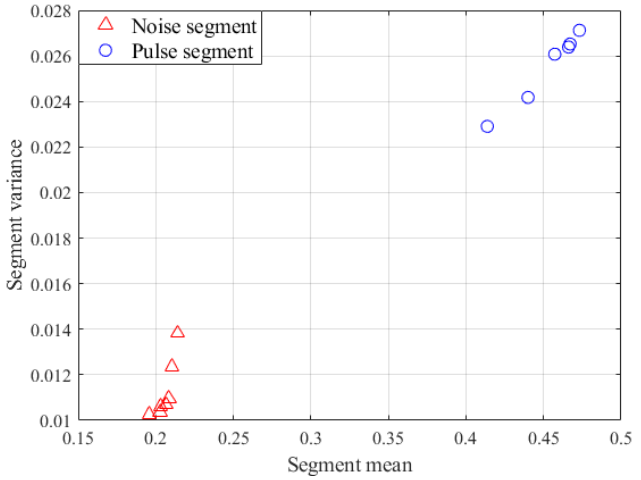

FIGURE 11. 2-D feature data after *K*-means algorithm.

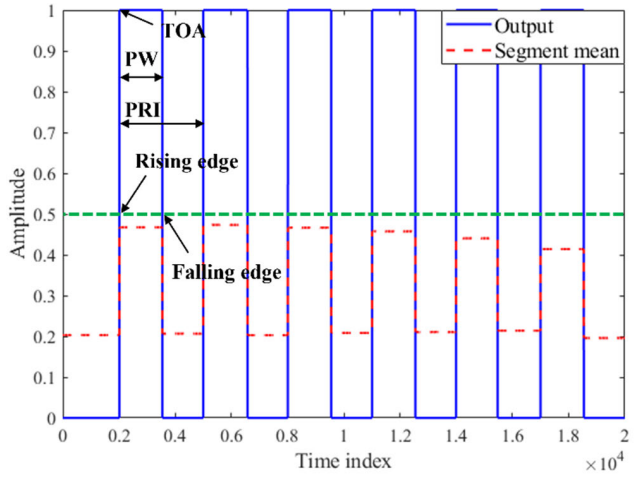

FIGURE 12. Output from the estimation with *K*-means.

First, we generate the feature data by converting the segment's mean and variance into a 2-D feature data. Second, we classify this 2-D data into pulse and noise segments by implementing the K-means algorithm, as shown in Fig. 11. Then, 1 and 0 are assigned to the segment's mean (or variance) value corresponding to the data of each noise and pulse cluster. Consequently, the output from this procedure has 1 for the pulse domain and 0 for the noise domain, as shown in Fig. 12. Because the outcome has 1 and 0, TOA, PW, and PRI can be estimated by applying the fixed criterion between 0 and 1 without any calculation for selecting the threshold. The output changes from 0 to 1 and 1 to 0 are denoted as rising and falling edges, respectively. Then, we can determine the parameters through the following process.

$$\begin{aligned} R &= [r(1)\, r(2) \cdots r(p)\, N], \\ F &= [f(1) f(2) \cdots f(p)], \\ TOA &= R(1) = r(1), \\ PW(i) &= F(i) - R(i), \\ PRI(i) &= R(i+1) - R(i), \end{aligned} \tag{12}$$

where R and F are rising and falling edges, p is the number of features classified into pulse segment, N is the end of the time index, and $i = 1, 2, \ldots, p$.

IV. PERFORMANCE EVALUATION

A. SIMULATION SETUP

In our experiment, we evaluated the estimation performance of the proposed method using MATLAB. The notations for the parameters are described in Table 2 and the experimental environments are given in Tables 3 and 4. For performance analysis of the TOA, PW, and PRI, we used root-mean-square-error (RMSE), and repeatedly generated each signal given in Table 3 500 times per SNR for RMSE calculation. For the convenience of simulation, we fixed the numbers of TOA samples, pulses, and sampling frequency to 2,000, 6, and 100 MHz, respectively, and randomly set the PRI of the generated signal to have four types having fixed values: constant, jitter, stagger, and Dwell and Switch (D&S), given in Table 5 [31]. The range of the SNR was −5 to 5 dB, and we observed an estimation error every 2 dB. We presumed the generated signal was collected after passing through the digital channelizer [32]. In addition, simulation was performed

TABLE 2. Notations for the signal generation and denoising.

Param.	Description
U	Uniform distribution
f_s	Sampling frequency
B	Signal bandwidth
N_p	The number of pulse samples
f_i	Frequency interval
L_c	Code length
cpp	The number of samples per cycle of the carrier frequency
M	The number of frequency steps
N_c	The number of the subcode in a code
f_c	Center frequency
CWT	Continuous wavelet transform
f_0	Initial center frequency of the sinc wavelet
B_0	Initial bandwidth of the sinc wavelet
α	Constant that determines the initial bandwidth and amplitude of the Gaussian wavelet
B_f	Filter bandwidth of the proposed method

TABLE 3. Parameters for the signal generation.

Radar waveform	Param.	Value
UM	N_p f_c [Hz]	U[512,1920] $U(f_s/6, f_s/5)$
LFM	B [Hz] N_p f_c [Hz]	$U(f_s/20, f_s/10)$ U[512,1920] $U(f_s/6, f_s/5)$
Costas	Costas array f_i [Hz] N_p	{1,4,2,3} $U(f_s/30, f_s/20)$ U[512,1920]
Barker	L_c cpp f_c [Hz]	{7,11,13} U(20,24) $U(f_s/6, f_s/5)$
Frank, P1	M cpp f_c [Hz]	{6,7,8} {3,4,5} $U(f_s/6, f_s/5)$
P2	M cpp f_c [Hz]	{6,8} {3,4,5} $U(f_s/6, f_s/5)$
P3, P4	N_c cpp f_c [Hz]	{36,49,64} {3,4,5} $U(f_s/6, f_s/5)$

under AWGN, and we assumed that the information about the mean and variance of AWGN could be known in advance when no signal was received.

TABLE 4. Parameters for the denoising.

Denoising	Param.	Value
CWT (sinc)	f_0 [Hz] B_0 [Hz] Filter bank type	$f_s/2 - B_0$ $f_s/50$ Overlap a half of the adjacent filter banks
CWT (Gaussian)	α Filter bank type	0.1 Equally spaced scaling factor
Proposed	B_f [Hz] Filter bank type ξ	$f_s/50$ Overlap a half of the adjacent filter banks 2
All	# of filter banks	100

TABLE 5. Parameters for the pulse repetition interval.

Type	Value
Constant	[30, 30, 30, 30, 30, 30] μs
Jitter	[26.9, 32.5, 29.2, 34.1, 27.5, 29.8] μs
Stagger	[25, 30, 35, 25, 30, 35] μs
D&S	[25, 25, 30, 30, 35, 35] μs

We compared the proposed method with the modified sinc wavelet and the Gaussian wavelet discussed in [33]. As these methods focused only on noise suppression, parameter estimation was not considered. We combined these wavelet transform-based methods with the proposed estimation step to analyze the performance under the same condition. In the proposed estimation step, the PELT detected abrupt mean changes, and we set the initial penalty range $[\beta_{min}, \beta_{max}]$ to [0.5, 6] and the interval β_{inter} to 0.1 for the mCROPS. The threshold in estimation with K-means was set to 0.5.

B. ESTIMATION RESULT

Fig. 13 represents the TOA, PW, and PRI estimation results for the unmodulated (UM) signal given in Table 3. The results for each parameter show similar patterns, and the estimation accuracy tends to increase as the SNR improves in all methods. Among them, the modified sinc wavelet and the proposed method have similar performance. This result indicates that the sinc wavelet suppresses the noise without distortion as the unmodulated signal has only a center frequency without bandwidth. However, in detail, the proposed method slightly outperforms the modified sinc wavelet. This result reflects that unnecessary thermal noise is included when the sinc wavelet bandwidth is larger than the signal bandwidth. In the case of the modified Gaussian wavelet, it is inferior to others as the filter gain is not flat.

Fig. 14 shows the TOA, PW, and PRI estimation results generated by calculating the average RMSE for the eight

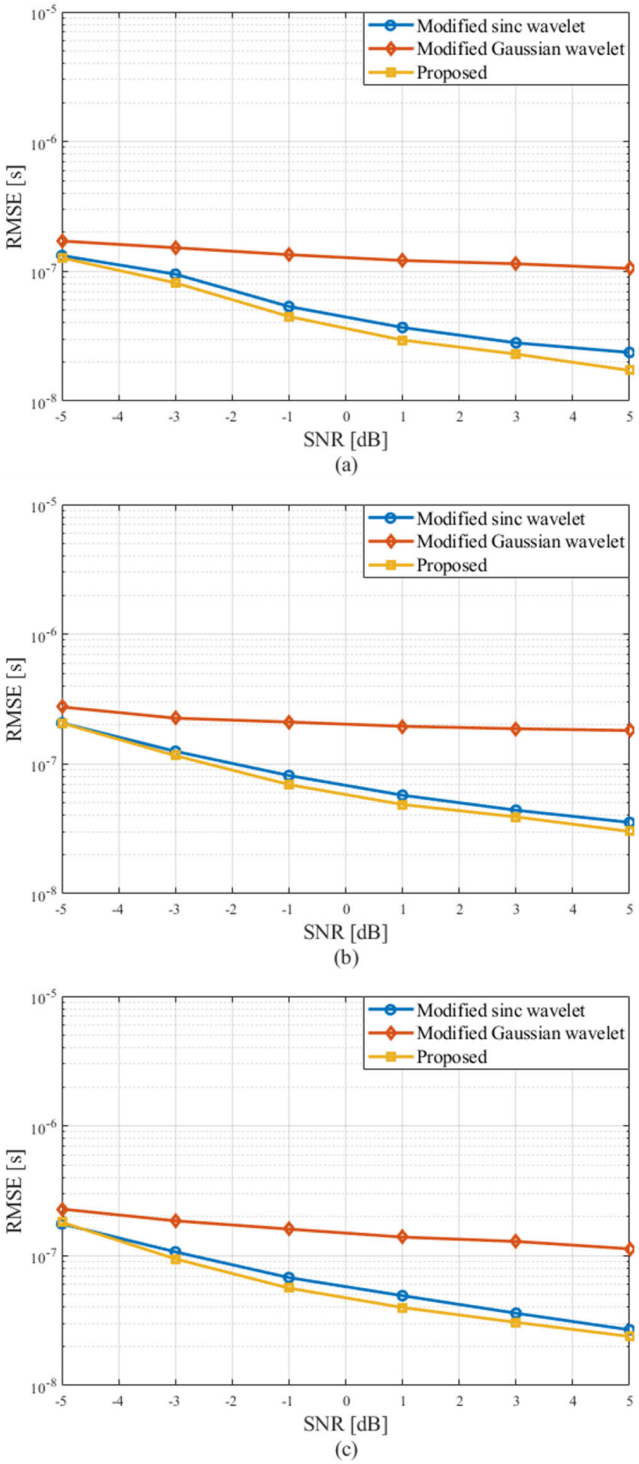

FIGURE 13. Estimation result for the parameters of the unmodulated signal; (a) time of arrival, (b) pulse width, (c) pulse repetition interval.

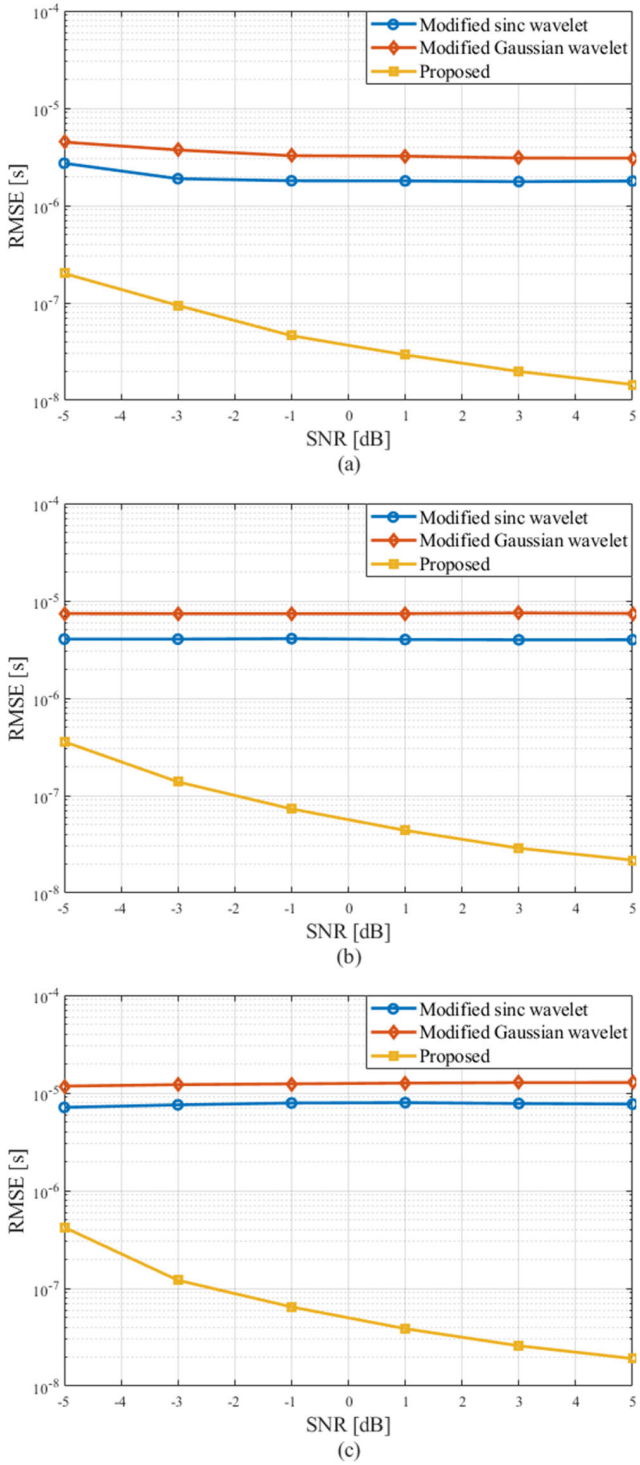

FIGURE 14. Estimation result for the parameters of the eight modulated signal; (a) time of arrival, (b) pulse width, (c) pulse repetition interval.

modulated signals considered in Table 3. The results for each parameter show a similar appearance as in Fig. 13. The proposed method decreases the estimation error as the SNR increases and generates remarkable results even in a weak-signal environment. However, unlike in Fig. 13, the estimation performance of the wavelet transform deteriorates. In addition, the RMSE is saturated regardless of the SNR. These results can be explained through Fig. 15, which shows the denoised pulse train produced from the modified sinc wavelet. The wavelet transform may distort the signal when the filter bandwidth is smaller than the signal bandwidth. Consequently, the denoised pulse train appears to have 12 pulses even though the original number of pulses is 6. Because of this distortion, it is difficult to distinguish between

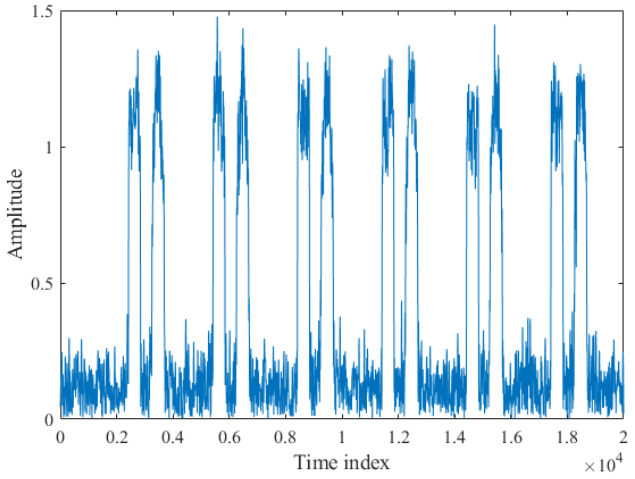

FIGURE 15. Distorted pulse train with six pulses obtained from the wavelet transform.

pulses and noise correctly, resulting in poor performance even when the SNR is increased. In contrast, the proposed method mitigates the noise without distortion by using a flexible filter bandwidth based on CPD-CP. In other words, the proposed method accurately estimates parameters for various modulation schemes and bandwidths in EW.

Additionally, we evaluated the estimation performance for the modulation bandwidth of the eight modulated signals considered in Table 3 using the CPD-CP. Each signal was generated 500 times per SNR, and we also used the RMSE for performance analysis. The modulation bandwidth ΔB can be determined by using the output of the CPD-CP as follows:

$$\Delta B = cp_{max} - cp_{min}. \tag{13}$$

Table 6 represents the estimation result of the modulation bandwidth. The RMSE in each SNR is about 1.3 MHz, which does not show an accurate estimation result. This is because the resolution of the time-frequency analysis produced by a sinc filter bank is low. In addition, as the power ratio is calculated by projecting the time-frequency analysis onto the frequency axis, the frequency resolution of the power ratio still remains to be low. Thus, the estimated bandwidth is slightly larger than the actual bandwidth. We may improve the frequency resolution by using other time-frequency analysis with a high resolution such as WVD or Choi–Williams distribution instead of a sinc filter bank. However, there is a trade-off between the performance and the computational complexity. As this paper focused on improving TOA, PW, and PRI estimation performance by reducing noise without distortion, we have not presented the applicable result for the estimation of the modulation bandwidth but will consider it in future work.

V. CONCLUSION

We proposed a TOA, PW, and PRI estimation method based on CPD by developing three key algorithms to estimate parameters for LPI radar pulse trains, not single pulses. The CPD-CP method was introduced to suppress the noise from signals with various modulation schemes and bandwidths without distortion. The mCROPS, which efficiently provides an adequate penalty constant for running PELT on a denoised pulse train, was presented. Finally, estimation with K-means was proposed for the authenticity of the estimation without considering the threshold calculation. The proposed method was compared with the existing wavelet transform-based method. The simulation results demonstrated that the proposed method precisely estimates the TOA, PW, and PRI even in the low SNR for various modulation schemes. In contrast, the existing wavelet transform may cause performance degradation by distorting the intercepted signal. Therefore, the proposed method is expected to be effectively utilized in ES systems. In future work, we plan to apply the proposed method to signal in a real environment.

TABLE 6. RMSE for the modulation bandwidth of the eight modulated signal.

SNR [dB]	-5	-3	-1	1	3	5
RMSE [MHz]	1.32	1.30	1.29	1.29	1.29	1.28

REFERENCES

[1] P. E. Pace, *Detecting and Classifying Low Probability of Intercept Radar*. Norwood, MA, USA: Artech House, 2004.
[2] D. C. Schleher, "LPI radar: Fact or fiction," *IEEE Aerosp. Electron. Syst. Mag.*, vol. 21, no. 5, pp. 3–6, May 2006.
[3] F. Hejazikookamari, Y. Norouzi, E. S. Kashani, and M. M. Nayebi, "A novel method to detect and localize LPI radars," *IEEE Trans. Aerosp. Electron. Syst.*, vol. 55, no. 5, pp. 2327–2336, Oct. 2019.
[4] X. Li, Z. Liu, and Z. Huang, "Deinterleaving of pulse streams with denoising autoencoders," *IEEE Trans. Aerosp. Electron. Syst.*, vol. 56, no. 6, pp. 4767–4778, Dec. 2020.
[5] S.-H. Kong, M. Kim, L. M. Hoang, and E. Kim, "Automatic LPI radar waveform recognition using CNN," *IEEE Access*, vol. 6, pp. 4207–4219, 2018.
[6] P. Sharma, K. K. Sarma, and N. E. Mastorakis, "Artificial intelligence aided electronic warfare systems-recent trends and evolving applications," *IEEE Access*, vol. 8, pp. 224761–224780, 2020.
[7] J. Matuszewski, "The analysis of modern radar signals parameters in electronic intelligence system," in *Proc. 13th Int. Conf. Modern Problems Radio Eng., Telecommun. Comput. Sci. (TCSET)*, Lviv, Ukraine, Feb. 2016, pp. 298–302.
[8] R. Wiley, *ELINT: The Interception and Analysis of Radar Signals*. Norwood, MA, USA: Artech House, 2006.
[9] N. U. kumar, V. Dhananjayulu, and V. A. Kumar, "Deinterleaving of radar signals and its parameter estimation in EW environment," *Int. J. Emerg. Technol. Adv. Eng.*, vol. 4, no. 9, pp. 490–494, Sep. 2014.
[10] B. M. Albaker and N. A. Rahim, "Signal acquisition and parameter estimation of radio frequency pulse radar using novel method," *IETE J. Res.*, vol. 55, no. 3, pp. 128–134, May 2009.
[11] A. A. Ahmad, S. Lawan, M. Ajiya, Z. Y. Yusuf, and L. M. Bello, "Extraction of the pulse width and pulse repetition period of linear FM radar signal using time-frequency analysis," *J. Adv. Sci. Eng.*, vol. 3, no. 1, pp. 1–8, May 2020.
[12] V. M. Duong, J. Vesely, P. Hubacek, P. Janu, and N. G. Phan, "Detection and parameter estimation analysis of binary shift keying signals in high noise environments," *Sensors*, vol. 22, no. 9, p. 3203, Apr. 2022.
[13] W. Tao, J. Kaili, L. Jingyi, J. Tingting, and T. Bin, "Research on LPI radar signal detection and parameter estimation technology," *J. Syst. Eng. Electron.*, vol. 32, no. 3, pp. 566–572, Jun. 2021.
[14] K. Ranney, K. Tom, D. Tadas, N. Tesny, A. Magill, and W. Diehl, "Magnitude-based pulse width estimation via efficient edge detection," *J. Appl. Remote Sens.*, vol. 16, no. 1, Feb. 2022, Art. no. 016509.
[15] Y. Lee, D. Kim, and H. Kim, "Enhanced pulse amplitude estimation for electronic warfare systems," *IET Radar, Sonar Navigat.*, vol. 13, no. 7, pp. 1123–1130, Jul. 2019.

[16] J. Tang, Z. Yang, and Y. Cai, "Wideband passive radar target detection and parameters estimation using wavelets," in *Proc. Rec. IEEE Int. Radar Conf.*, Alexandria, VA, USA, May 2000, pp. 815–818.
[17] J.-W. Shin, K.-H. Song, K.-S. Yoon, and H.-N. Kim, "Weak radar signal detection based on variable band selection," *IEEE Trans. Aerosp. Electron. Syst.*, vol. 52, no. 4, pp. 1743–1755, Aug. 2016.
[18] E. S. Page, "Continuous inspection schemes," *Biometrika*, vol. 41, nos. 1–2, pp. 100–115, Jun. 1954.
[19] G. Chen, G. Lu, W. Shang, and Z. Xie, "Automated change-point detection of EEG signals based on structural time-series analysis," *IEEE Access*, vol. 7, pp. 180168–180180, 2019.
[20] Z. Harchaoui, F. Vallet, A. Lung-Yut-Fong, and O. Cappe, "A regularized kernel-based approach to unsupervised audio segmentation," in *Proc. IEEE Int. Conf. Acoust., Speech Signal Process. (ICASSP)*, Taipei, Taiwan, Apr. 2009, pp. 1665–1668.
[21] M. A. Richards, J. A. Scheer, and W. A. Holm, *Principles of Modern Radar: Basic Principles*. Raleigh, NC, USA: SciTech, 2010.
[22] M. I. Skolnik, "Introduction to radar," in *Radar Handbook*, vol. 2. New York, NY, USA: McGraw-Hill, 1962.
[23] C. Truong, L. Oudre, and N. Vayatis, "Selective review of offline change point detection methods," *Signal Process.*, vol. 167, Feb. 2020, Art. no. 107299.
[24] R. Maidstone, T. Hocking, G. Rigaill, and P. Fearnhead, "On optimal multiple changepoint algorithms for large data," *Statist. Comput.*, vol. 27, no. 2, pp. 519–533, Mar. 2017.
[25] R. Killick, P. Fearnhead, and I. A. Eckley, "Optimal detection of change-points with a linear computational cost," *J. Amer. Statist. Assoc.*, vol. 107, no. 500, pp. 1590–1598, 2012.
[26] K. Haynes, I. A. Eckley, and P. Fearnhead, "Computationally efficient changepoint detection for a range of penalties," *J. Comput. Graph. Statist.*, vol. 26, no. 1, pp. 134–143, Jan. 2017.
[27] P. Flach, *Machine Learning: The Art and Science of Algorithms That Make Sense of Data*, Cambridge, U.K.: Cambridge Univ. Press, 2012.
[28] N. Ehara, I. Sasase, and S. Mori, "Weak radar signal detection based on wavelet transform," in *Proc. IEEE Int. Conf. Acoust., Speech Signal Process.*, Adelaide, SA, USA, Apr. 1994, pp. 377–380.
[29] D. Adamy, *EW 101: A First Course in Electronic Warfare*. Norwood, MA, USA: Artech House, 2001.
[30] P. Fearnhead, R. Maidstone, and A. Letchford, "Detecting changes in slope with an L0 penalty," *J. Comput. Graph. Statist.*, vol. 28, no. 2, pp. 265–275, Apr. 2019.
[31] S. Wei, Q. Qu, Y. Wu, M. Wang, and J. Shi, "PRI modulation recognition based on squeeze-and-excitation networks," *IEEE Commun. Lett.*, vol. 24, no. 5, pp. 1047–1051, May 2020.
[32] W. Namgoong, "A channelized digital ultrawideband receiver," *IEEE Trans. Wireless Commun.*, vol. 2, no. 3, pp. 502–510, May 2003.
[33] J.-H. Bang, D.-H. Park, and H.-N. Kim, "Improved TOA and pulse width estimation for wideband signal in electronic warfare systems," in *Proc. 19th Eur. Radar Conf. (EuRAD)*, Milan, Italy, Sep. 2022, pp. 73–76.

JONG-HYEON BANG (Graduate Student Member, IEEE) received the B.S. degree in electronic engineering from Pusan National University, Busan, South Korea, in 2021, where he is currently pursuing the M.S. degree in electrical and electronics engineering. His research interests include radar signal processing and electronic warfare systems.

DO-HYUN PARK (Graduate Student Member, IEEE) received the B.S. degree in electronic engineering from Pusan National University, Busan, South Korea, in 2019, where he is currently pursuing the integral master's and Ph.D. degrees in electrical and electronics engineering. His primary research interests include radar signal processing, array signal processing, electronic warfare systems, and deep learning.

WONJIN LEE was born in Kimpo, South Korea, in 1973. He received the B.Eng. degree in control and measurement engineering from Korea University, South Korea, in 1999. In 2002, he joined the Electronic Warfare Research and Development Laboratory, LIG Nex1, South Korea. His research interests include digital receiver and digital signal processing and time synchronization.

DOOHWAN KIM was born in Incheon, South Korea, in 1989. He received the B.S. degree in electronic engineering from Soongsil University, South Korea, in 2017. In 2017, he joined the Electronic Warfare Research and Development Laboratory, LIG Nex1, South Korea. His research interests include digital receiver and digital signal processing and jamming.

HYOUNG-NAM KIM (Member, IEEE) received the B.S., M.S., and Ph.D. degrees in electronic and electrical engineering from the Pohang University of Science and Technology, Pohang, South Korea, in 1993, 1995, and 2000, respectively. From 2000 to 2003, he was with the Electronics and Telecommunications Research Institute, Daejeon, South Korea, developing advanced transmission and reception technology for terrestrial digital television. In 2003, he joined as a Faculty Member of the Department of Electronics Engineering, Pusan National University, Busan, South Korea, where he is currently a full-time Professor. From 2009 to 2010, he was with the Department of Biomedical Engineering, The Johns Hopkins University School of Medicine, as a Visiting Scholar. From 2015 to 2016, he was a Visiting Professor with the School of Electronics and Computer Engineering, University of Southampton, U.K. His research interests include radar/sonar signal processing, machine learning, adaptive filtering, biomedical signal processing, digital communications, electronic warfare support systems, and brain–computer interfaces. He is a member of IEIE and KICS.